JOURNAL OF AIRCRAFT
Vol. 46, No. 1, January–February 2009

Thickness Effect on the Thrust Generation of Heaving Elliptic Airfoils

Sangjoon An* and Joosung Maeng†
Hanyang University,
Seoul 133-791, Republic of Korea
and
Cheolheui Han‡
Chungju National University,
Chungju 143-701, Republic of Korea

DOI: 10.2514/1.37903

The influence of the Reynolds number on the propulsive characteristics of insect wings is investigated by focusing on the aerodynamic transition from drag to thrust. The effect of both the thickness ratio and the Reynolds number on the thrust generation of elliptic airfoils is investigated using a lattice Boltzmann method. Three Reynolds numbers ($Re = 50$, 100, and 185) and two Strouhal numbers ($Sr = 0.2$ and 0.4) are treated, while the thickness ratio is varied from 0.05 to 1.0. For all investigated Reynolds numbers, it is found that the airfoils oscillating at $Sr = 0.2$ do not produce thrust. For $Sr = 0.4$, it is found that thrust is produced at $Re = 185$. It is found that an airfoil of approximately 10% thickness produces maximum thrust. Thus, it can be said that, for thrust generation, there exists critical Reynolds and Strouhal numbers, and the thickness ratio is also a crucial parameter. By investigating the vortex pattern, velocity profiles, and vorticity intensities of the vortex cores behind the oscillating airfoils, it is found that 1) mushroom vortex patterns indicative of thrust do not completely guarantee the thrust generation, and 2) a phase lag between the thrust-force indicating vortex pattern and the resulting thrust production is observed. The present investigation shows that thrust-producing airfoils should produce strong vortices, enough to overcome the momentum deficit due to the boundary layer. Present results are obtained within the limitation of the laminar flow assumption.

Nomenclature

c = lattice speed
C_D = drag coefficient, $C_D = 2F_x/\rho D_x U^2$
c_s = speed of sound
D_x = x-directional elliptic foil, or circular cylinder, diameter
D_y = y-directional elliptic foil diameter
$\mathbf{e}$ = particle velocity in a lattice Boltzmann equation model
$\mathbf{e}_i$ = discrete particle velocity in a lattice Boltzmann equation model
f = single particle mass distribution function
f = postcollision distribution function
f_e = oscillation frequency of cylinder, or elliptic foil
f_o = natural shedding frequency for a stationary cylinder
f^{eq} = local equilibrium distribution function
h = amplitude of oscillation
k = reduced frequency, $k = 2\pi f_e \cdot D_x/U$
p = pressure
Q = collision operator
Re = Reynolds number, $Re = U \cdot D_x/v$
Sr = Strouhal number, $Sr = f_e \cdot h/U$
t = lattice time
U = flight speed
w_i = weighting factor
x, y = Cartesian coordinates
x_b = solid lattice node
x_f = fluid lattice node
y_c = y-directional center position of elliptic foil, $y_c = h \cdot \sin\omega \cdot t$
Δ = unit lattice length
δ = distance between fluid node and boundary of elliptic foil, or cylinder
ν = kinematic viscosity
ρ = density
τ = relaxation parameter for collision
ω = angular velocity

Received 5 April 2008; revision received 25 August 2008; accepted for publication 31 August 2008.

*Graduate Assistant, School of Mechanical Engineering, 17 Haengdang Dong, Seong dong Gu.
†Professor, School of Mechanical Engineering, 17 Haengdang Dong, Seong dong Gu.
‡Assistant Professor, Department of Aeronautical and Mechanical Design Engineering, 123 Geom-Dan Ri, Iryu Myeon, Chungju, Chungchungbuk Do. Member AIAA.

I. Introduction

THE aerodynamics and kinematics of insect flight have received significant attention by biologists over the past decades. In regard to the development of a micro air vehicle, insect flight has been of considerable interest to the aerospace engineering community. For hovering or cruise flight, considerable progress has been achieved for elucidating the relationship between wing kinematics and lift generation mechanisms. In addition to the increased practicality of computational fluid dynamics, this progress has been based on advanced flow visualization technology, which uses a high-speed camera and a digital particle image velocimetry to study the flow. Extensive reviews on flapping foils and their applications to the development of aerial or marine vehicles are given by Rozhdestvensky and Ryzhov [1] and Ho et al. [2]. Notable discussions concerning the lift generation mechanisms of insect wings are present in [3–6], and extensive reviews on the subject are also presented in several books [7–9].

Another aspect of flapping wing aerodynamics is the control of vortices for the purpose of propulsion. Extensive reviews on this subject are presented with regard to the enhancement of man-made

propulsors [1,10,11]. The study of thrust generation for flapping wings or fins was first initiated by Knoller [12] and Betz [13]. They observed that a positive thrust component is generated during both the up and down strokes of a flapping wing. Birnbaum [14] found that the effect of vortex shedding from the airfoil trailing edge is governed by two characteristic speeds [flapping velocity ($f_e D_x$) and flight speed (U)], and introduced a reduced frequency of $k = 2\pi f_e D_x/U$. Thus, the Strouhal number ($Sr = f_e h/U$), which influences the frequency, location, and orientation of the vortex shedding, is also a critical parameter for thrust generation. Von Kármán and Burgers [15] discovered that the drag (or thrust) generation is a function of the location and orientation of the shed wake vortices. When the Strouhal number becomes larger than a certain value, the shed wake from the airfoil's trailing edge produces a staggered array of vortices, with rotations opposite of those from a von Kármán vortex street, which induce jetlike flows [16,17]. According to the experimental study of Lai and Platzer [18], mushroom-shaped vortices that point upstream indicate a drag-producing wake, whereas mushroom-shaped vortices that point downstream indicate a thrust-producing wake. Platzer and Jones [19] show that the formation and evolution of unsteady reverse von Kármán vortex streets is fundamentally dependent on the value of $kh(=2\pi Sr)$.

Recently, the influence of the Reynolds number on the aerodynamic characteristics of insect wings has been revealed by investigating the change in the lift. Wang [20] investigated the aerodynamic characteristics of flapping two-dimensional wings and found that the lift coefficient decreases with a decreasing Reynolds number. Wu and Sun [21] found from a three-dimensional simulation that, when the Reynolds number decreases, the lift coefficient decreases and the drag coefficient increases. Wu and Sun also found that the drag increases for Reynolds number values below 100. Miller and Peskin [22] investigated the changes in lift and vortex dynamics for Reynolds numbers between 8 and 128. They found that aerodynamic transition is observed for Reynolds number values between 32 and 64. Also, they observed that formed vortices did not shed during translation at Reynolds number values less than 32, whereas they alternatively shed during translation at Reynolds number values above 64. Furthermore, they determined that lift is not generated below a critical Reynolds number [22]. Similarly, Walker [23] observed that both leading and trailing edge vortices are not formed below a critical Reynolds number. Shyy et al. [9] and Shyy and Liu [24] investigated the effect of Reynolds numbers on the attached leading edge vortex.

With respect to the thrust generation, Childress and Dudley [25] studied the swimming of the Clionidae and found that it alternated its mode of locomotion, between ciliary and flapping modes, depending on the hydromechanical environment [25] and Reynolds number. Godoy–Diana et al. [26] also investigated the relation between the thrust generation and wake pattern of a flapping foil. They found that there exists a phase lag between the wake pattern and the thrust generation.

The purpose of this paper is to investigate, using a laminar lattice Boltzmann method, the effect of thickness on the aerodynamic transition in the drag produced by airfoils oscillating in a low Reynolds number flow. The shape of an airfoil is a major design parameter in the aircraft of a wing. Most of the previous experimental and numerical studies of unsteady airfoils, with the exception of the study by Lentink and Gerritsma [27], assume an airfoil shape equal to a thin ellipse or a flat plate. For example, Sun and Tang [28] studied a 12% thick ellipse, whereas Wang [29] and Freymuth et al. [30] studied a 10% thick ellipse. According to Lai and Platzer [18], who compared the velocity profiles generated by an airfoil and a circular cylinder in a plunging motion, a circular cylinder does not produce a jet flow, whereas an airfoil does as a result of its curvature and asymmetry. The effect of airfoil thickness on this jet flow has not been studied previously. Thus, in this paper the airfoil shape is changed from a circular cylinder to a thin ellipse, while the Reynolds number is changed from 50 to 270 in order to investigate the thrust generation. The Strouhal number is varied between 0.2 and 0.4 for the present study, which replicates the values for animal flight in nature [31]. The present method is validated by comparing the computed aerodynamic characteristics with other numerical results based on the Navier–Stokes (N–S) equations.

II. Lattice Boltzmann Method

The lattice Boltzmann equation (LBE) is a derivative of lattice gas automata. LBM can deal with fluid dynamics from the microscopic, kinetic level to the macroscopic fluid dynamic behavior by describing the evolution of the velocity distribution function on a lattice. The particle interpretation of the scheme with a particle streaming step followed by a collision step allows the easy parallel implementation for complex geometries on massively parallel computers.

The Boltzmann equation is represented as

$$\frac{\partial f}{\partial t} + \mathbf{e} \cdot \nabla f = Q \tag{1}$$

In Eq. (1), both the left- and right-hand sides represent streaming and collision processes, respectively. The Boltzmann equation can be simplified with BGK (Bhatnagar–Gross–Krook) approximation [32], resulting in the replacement of the nonlinear collision operator Q by a linearized collision term with the Maxwell equilibrium distribution function f^{eq}

$$\frac{\partial f}{\partial t} + \mathbf{e} \cdot \nabla f = -\frac{1}{\tau}(f - f^{\mathrm{eq}}) \tag{2}$$

where τ is the relaxation time for collision. Then, the BGK lattice Boltzmann equation is represented as an explicit form that is easy to implement and straightforward to parallelize.

$$f_i(\mathbf{x} + \mathbf{e}_i \delta t, t + \delta t) - f_i(\mathbf{x}, t) = -\frac{1}{\tau}[f_i(\mathbf{x}, t) - f^{\mathrm{eq}}(\mathbf{x}, t)] \tag{3}$$

When the D2Q9 model [33] shown in Fig. 1 is applied to Eq. (3), the discrete velocity set $\mathbf{e}_i$ becomes

$$\begin{aligned} &c(0,0) && && i = 0 \\ &c(\cos\theta_i, \sin\theta_i), && \theta_i = (i-4)\pi/2, && i = 1-4 \\ &\sqrt{2}c(\cos\theta_i, \sin\theta_i), && \theta_i = (i-4)\pi/2 + \pi/2, && i = 5-8 \end{aligned} \tag{4}$$

where the subscript i represents the direction of each discrete velocity. The lattice speed c represents $\delta x/\delta t$.

The expansion of equilibrium distribution f_i^{eq} in a Taylor series of $\mathbf{u}$ up to second-order results in

$$f_i^{\mathrm{eq}} = w_i \rho \left[1 + 3\frac{\mathbf{e}_i \cdot \mathbf{u}}{c^2} + \frac{9}{2}\frac{(\mathbf{e}_i \cdot \mathbf{u})^2}{c^4} - \frac{3}{2}\frac{\mathbf{u} \cdot \mathbf{u}}{c^2} \right] \tag{5}$$

where w_i represents the weighting factor whose values depend on the discrete velocity set

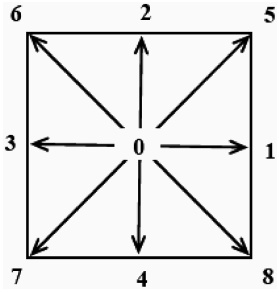

Fig. 1 Two-dimensional, nine-velocity lattice Boltzmann model (D2Q9 model).

$$w_i = \begin{cases} 4/9, & i = 0 \\ 1/9, & i = 1-4 \\ 1/36, & i = 5-8 \end{cases} \tag{6}$$

The lattice Boltzmann method is solved with the following two steps:

$$\text{Collision step}: \widehat{f}_i(\mathbf{x}, t) = f_i(\mathbf{x}, t) - \frac{1}{\tau}[f_i(\mathbf{x}, t) - f^{\text{eq}}(\mathbf{x}, t)] \tag{7a}$$

$$\text{Streaming step}: f_i(\mathbf{x} + \mathbf{e}_i\delta t, t + \delta t) = \widehat{f}_i(\mathbf{x}, t) \tag{7b}$$

where $\widehat{f}_i$ represents the state after the collision. The Chapman–Enskog expansion [34], which is a standard multiscale expansion with time and space, results in the corresponding viscosity in the N–S equation

$$\nu = \left(\tau - \frac{1}{2}\right)c_x^2\delta t \tag{8}$$

In all LBE computations, τ must be larger than 0.5. The macroscopic quantities such as density and velocity can be obtained as

$$\rho = \sum_{i=0}^{8} f_i \tag{9}$$

$$\mathbf{u} = \frac{1}{\rho}\sum_{i=0}^{8} f_i\mathbf{e}_i \tag{10}$$

The speed of sound is $c_s = c/\sqrt{3}$ and the equation of state for an ideal gas is $p = \rho \cdot \mathcal{C}_S^2$.

A moving boundary condition [35] is employed in order to simulate airfoils in heave oscillation. The moving boundary condition that represents no-slip conditions on the curved boundary surface is

$$f_{\bar{i}}(\mathbf{x}, t) = q(1+2q)f_i(\mathbf{x} + \mathbf{e}_i\delta t, t) + (1-4q^2)f_{\bar{i}}(\mathbf{x}, t) - q(1-2q)f_{\bar{i}}(\mathbf{x} - \mathbf{e}_i\delta t, t) + 6w_i(\mathbf{e}_i \cdot \mathbf{u}_w), \qquad q < \frac{1}{2} \tag{12a}$$

$$f_{\bar{i}}(\mathbf{x}, t) = \frac{1}{q(2q+1)}f_i(\mathbf{x} + \mathbf{e}_i\delta t, t) + \frac{(2q-1)}{q}f_{\bar{i}}(\mathbf{x} - \mathbf{e}_i\delta t, t) - \frac{(2q-1)}{(2q+1)}f_{\bar{i}}(\mathbf{x} - 2\mathbf{e}_i\delta t, t) + \frac{6w_i}{q(2q+1)}(\mathbf{e}_i \cdot \mathbf{u}_w), \qquad q \geq \frac{1}{2} \tag{12b}$$

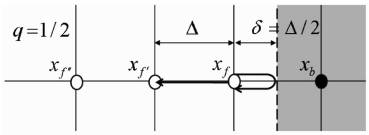

a) Simple bounce back condition (half-grid)

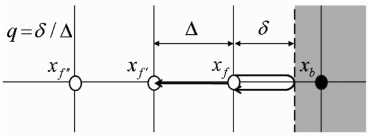

b) Revised bounce back condition (midgrid)

Fig. 2 Nomenclature of the implementation of the bounce back boundary condition on the solid wall (modified from Fig. 2 in [35]).

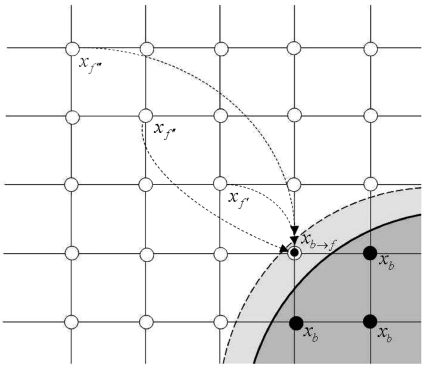

Fig. 3 Nomenclature of the extrapolation scheme (modified from Fig. 3 in [35]).

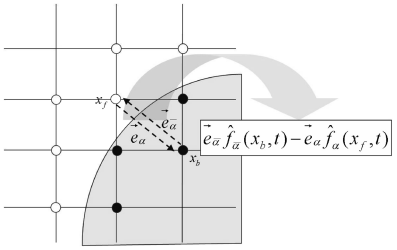

Fig. 4 Nomenclature of the momentum exchange scheme where the circle represents fluid nodes and the solid circle represents solid nodes (modified from Fig. 3 in [36]).

where $f_{\bar{\alpha}}$ is the distribution function of the velocity $\mathbf{e}_{\bar{i}}(\equiv -\mathbf{e}_i)$, $\mathbf{u}_w$ is the wall velocity of the moving foil, and q defines the fraction in the fluid region of a grid spacing intersected by the boundary (See Fig. 2 for nomenclature). When a solid point changes into a fluid point, the new fluid distribution function (f_{x_f}) is determined by using a second-order extrapolation along the direction of a chosen discrete velocity $\mathbf{e}_\alpha$. The discrete velocity set is chosen to maximize the quantity $\mathbf{n} \cdot \mathbf{e}_\alpha$, where $\mathbf{n}$ represents the out-normal to the wall. Then, the new distribution function can be given as follows (see Fig. 3 for the nomenclature):

$$f_{x_f} = 3f_{x_f'} - 3f_{x_f''} + f_{x_f'''} \tag{13}$$

The body forces on the body surface can be obtained by using a momentum exchange method [36]. The force on each link between fluid and solid nodes on the boundary can be represented with the amount of momentum exchange $\mathbf{e}_{\bar{\alpha}}\widehat{f}_{\bar{\alpha}}(x_b, t) - \mathbf{e}_\alpha\widehat{f}_\alpha(x_f, t)$ between two opposing directions of neighboring lattices illustrated in Fig. 4. The total fluid force acting on a solid body is obtained as

$$\mathbf{F}(x_b) = \sum_{\text{all}x_b}\sum_{\alpha=1}^{8} \mathbf{e}_\alpha[\widehat{f}_{\bar{\alpha}}(x_b, t) + \widehat{f}_\alpha(x_f, t)] \cdot [1 - w(x_b + \mathbf{e}_\alpha)] \tag{14}$$

where $w(x_b + \mathbf{e}_\alpha)$ is 0 at x_f and 1 at x_b. In Eq. (14), the inner summation integrates the momentum exchange between a solid node and all possible neighboring fluid nodes surrounding the solid node. The outer summation calculates the force contributed by all solid boundary nodes neighboring with fluid nodes [36].

III. Results and Discussion

To validate the fidelity of the present method for predicting the aerodynamic forces and vortex dynamics induced by the unsteady forced motion of a solid body, an unsteady flow problem of a circular cylinder in heaving oscillation in a free stream is selected [37,38]. In the present calculation, the Reynolds number based on the cylinder diameter is 185. The cylinder is given by a harmonic oscillation of $y_c = h\cos(2\pi f_e t)$, where y_c is the location of the cylinder center (see

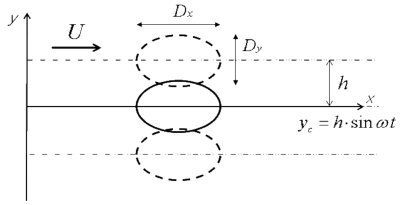

Fig. 5 Nomenclature of the present study.

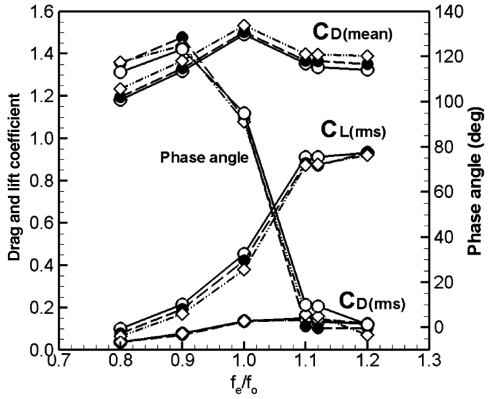

Fig. 6 Force coefficients and phase angles for $Re = 185$ and $h/D = 0.2$. Time-averaged values of C_d and C_d-bar, and root mean square (rms) values of C_d and C_l; phase angle between C_l and vertical position of the cylinder. (○: present, □: Kim and Choi [38], ●: Guilmineau and Queutey [37])

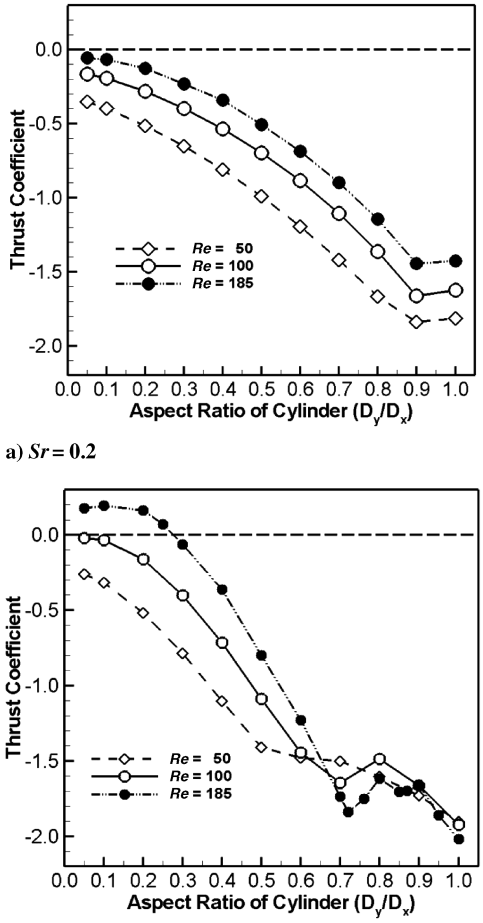

Fig. 7 Change in time-averaged thrust coefficient due to the variation of the thickness ratio (Dy/Dx).

Fig. 5 for the nomenclature). Both h and f_e are the amplitude and the frequency of the heave oscillation, respectively. The present computation is performed for $h/d = 0.2$ and $0.8 \leq f_e/f_0 \leq 1.2$ by following the given conditions in [37]. The natural frequency f_0 of vortex shedding behind a stationary cylinder and the time-averaged drag coefficient C_D of the cylinder are computed as 0.19 and 1.283, respectively. The number of grid points is 1200×1000 in the streamwise (x) and transverse (y) directions, respectively. As shown in Fig. 6, the computed variations of both force coefficients and phase angles with respect to the frequency ratio f_e/f_0 agree with the published results [37,38].

The effect of the change in the thickness ratio of an elliptic airfoil on the thrust generation is investigated for two Strouhal numbers ($Sr = 0.2$ and 0.4) and three Reynolds numbers ($Re = 50$, 100, and 185). The thickness ratio is controlled by changing the aspect ratio of the elliptic cylinder Dy/Dx. Figure 7 shows the change in the time-averaged drag (or thrust) coefficient. Both Figs. 8 and 9 represent the wake patterns and the velocity profiles behind the oscillating airfoils, respectively.

Figure 7 shows that the time-averaged drag coefficient of the elliptic foil decreases with the thickness ratio stepping down. When the thickness ratio is large ($Dy/Dx \geq 0.9$ at $Sr = 0.2$ and $Dy/Dx \geq 0.7$ at $Sr = 0.4$), the change in the time-averaged drag coefficient behaves like a bluff body. Vortex dynamics and resulting force changes have been a long time topic of bluff body aerodynamics that is beyond the scope of the present study. The aerodynamic transition from drag to thrust is observed when the Reynolds number is 185 and Dy/Dx is approximately less than 0.27 (an approximately 10% thick airfoil at $Re = 185$ and $Sr = 0.4$ produces the maximum thrust). It can be concluded from the figures that there are critical values of Reynolds and Strouhal numbers indicating whether the generated force is thrust or drag [25]. It can be also said that the slightly thick airfoils outperform the thin airfoils in the thrust generation.

Figure 8 shows the vorticity contours behind the oscillating airfoils at $Re = 185$($Sr = 0.2$ for Fig. 8a and St $= 0.4$ for Fig. 8b). As shown in Fig. 8a, the nascent wake vortices shed from both upper and lower surfaces of the circular airfoil ($Dy/Dx = 1.0$) are aligned into a staggered fashion (von Kármán vortex streets). As the thickness ratio decreases ($Dy/Dx = 0.9$), the distance between the upper and lower rows is reduced with alternating signs positioned in a row, and the mushroom vortex pattern indicative of drag starts quickly [19]. When the thickness ratio is less than 0.8, the mushroom vortex pattern indicative of drag changes into reverse von Kármán vortex streets with the distance between the upper and lower rows widening again. It is noticeable that the thrust is not generated even with thrust-indicating mushroom vortex patterns in the previous studies [16–18]. As shown in Fig. 8b, in the case of $Dy/Dx = 1.0$, typical von Kármán vortex streets with a drag-indicating mushroom vortex pattern are observed in the far field region after the complicated wake–wake interactions in the nascent region. When Dy/Dx is within the range from 0.8 to 0.9, the common feature of vorticity dynamics of the bluff body (irregular vortex patterns) becomes dominant in a few chord lengths behind the airfoil. In the case of $Dy/Dx = 0.7$, a mushroom vortex pattern [18] with its orientation pointing vertically downward is shown in the nascent region, and then the irregular vortex patterns dominates the fields again. When the thickness ratio is reduced further, except the nascent region where the thrust-indicating mushroom vortex pattern is observed, the mushroom vortex pattern is neutral with the mushroom head pointing vertically upward. As the thickness ratio is reduced further ($Dy/Dx \leq 0.4$), the neutral vortex pattern is changed into the mushroom vortex pattern indicative of thrust with its orientation pointing downward (thrust-producing wake pattern).

From the aerodynamic forces and wake patterns for $Re = 185$ as shown in the figures of Figs. 7 and 8, two questions arise 1) Why can the 10% thick airfoil at $Sr = 0.2$ not produce thrust even with the mushroom vortex pattern indicative of thrust; and 2) Why is there a phase lag between the wake pattern and the resulting force as is observed in the case of the 40% thick airfoil at $Sr = 0.4$. The qualitative answers can be given by looking at the time-averaged

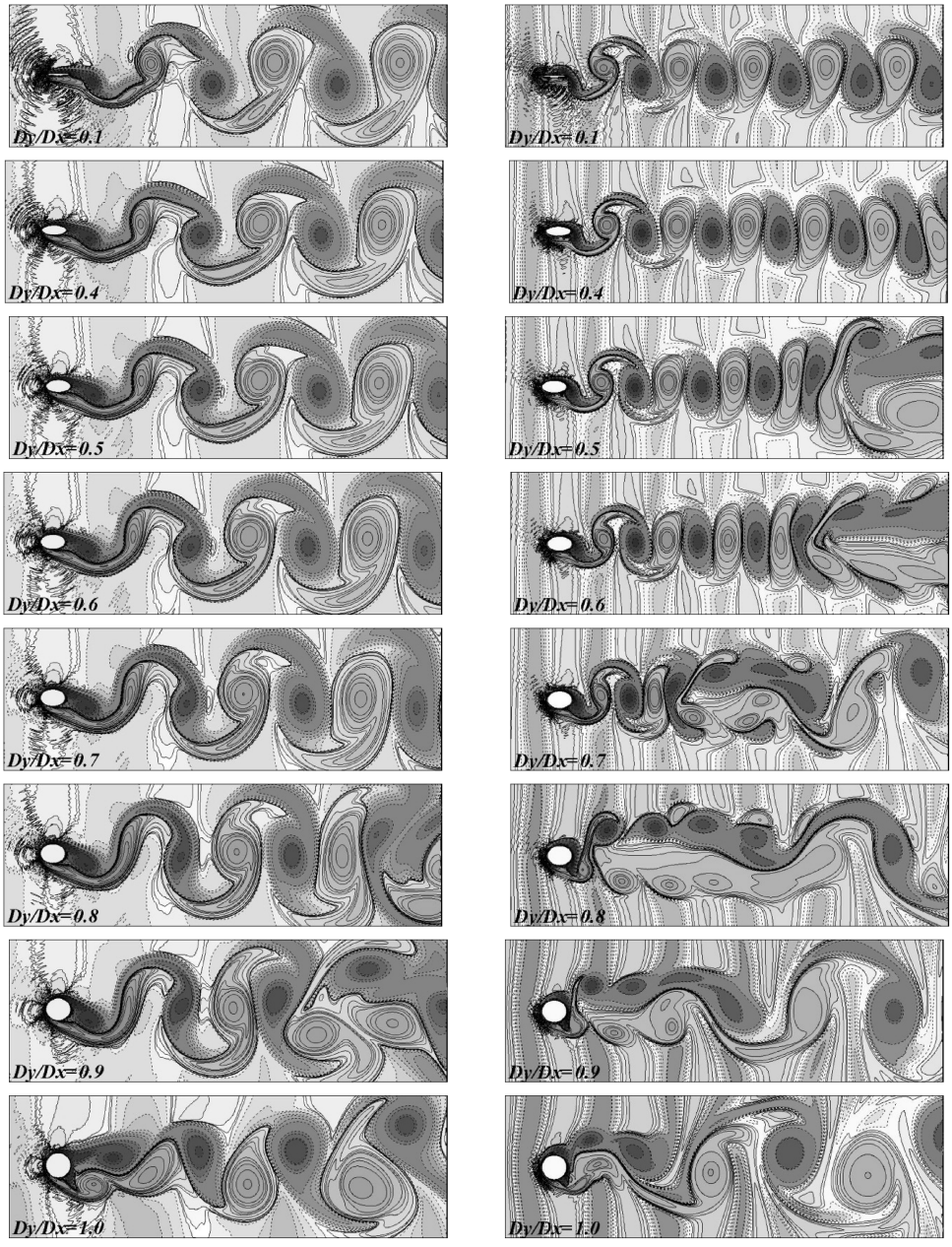

a) $Sr = 0.2$ b) $Sr = 0.4$

Fig. 8 Vorticity contours behind heaving airfoils for $Re = 185$.

velocity profiles and the vorticity intensities of the wake vortices behind the oscillating airfoils in Figs. 9 and 10. The time-averaged velocity profiles represent the momentum balance between the inlet and the outlet of the fluid domain. As shown in Figs. 9a and 9b, the velocity profile behind thick airfoils in heave oscillation show the typical drag-producing velocity profile. As the thickness ratio is reduced, the jet profile on the centerline with the velocity deficit peaks on either side of the centerline is observed. In case of $Sr = 0.2$,

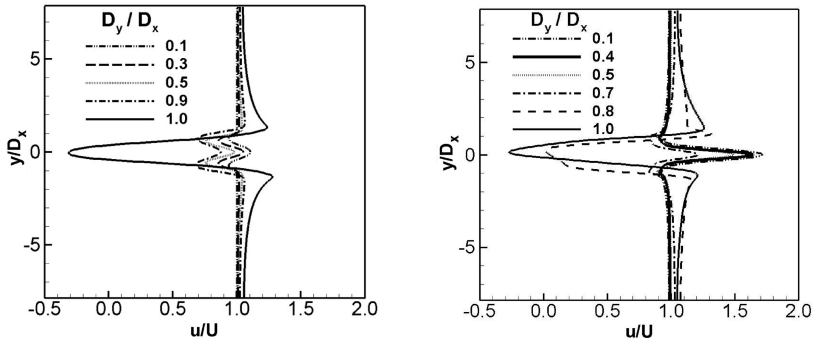

a) $Sr = 0.2$ b) $Sr = 0.4$

Fig. 9 Time-averaged velocity profiles behind heaving airfoils at $Re = 185$.

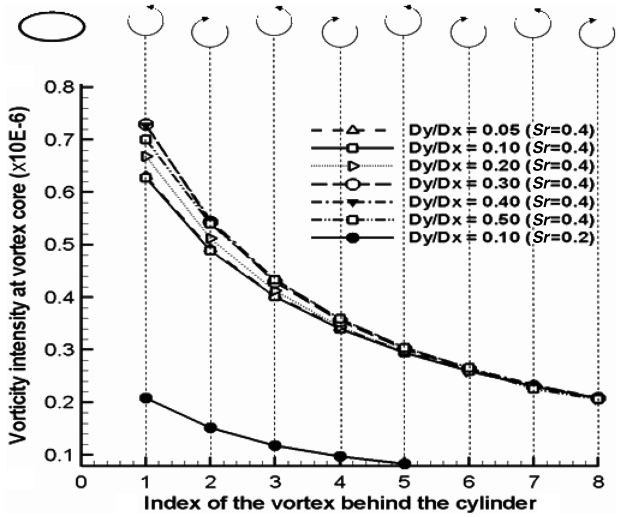

Fig. 10 Vorticity intensities at the vortex cores at $Re = 185$.

the jet is not strong enough to overcome the momentum deficit due to the boundary layer. When $Sr = 0.4$ and $Dy/Dx \leq 0.4$, the typical thrust-producing velocity profiles are observed with strong jet profiles on the centerline. The vorticity intensities in the vortex cores behind airfoils oscillating at both $Sr = 0.2$ and $Sr = 0.4$ explains the observed phase lag between the indicating vortex pattern and the resulting force generation. The intensities of vortices behind the thin foil oscillating at $Sr = 0.2$ are weaker than those behind thick airfoils oscillating at $Sr = 0.4$. Thus, it can be deduced that the thrust-producing airfoil should generate strong enough vortices to overcome the momentum deficit. The authors found that the conclusion in [26] agrees with our reasoning on the existence of the phase lag between the resulting force generation and the indicating vortex pattern.

IV. Conclusions

The present study investigated the effect of the thickness ratio on the thrust generation of the elliptic airfoils. Three Reynolds numbers ($Re = 50$, 100, and 185) and two Strouhal numbers ($Sr = 0.2$ and 0.4) are treated, and the thickness ratio varies from 0.05 to 1.0.

For the three given Reynolds numbers, the airfoils oscillating at $Sr = 0.2$ do not produce thrust. When $Sr = 0.4$, airfoils with $Dy/Dx \leq 0.4$ produce thrust at $Re = 185$. Thus, it can be said that, in a low Reynolds number flow, there exist critical Reynolds and Strouhal numbers for the thrust generation. An approximately 10% thick airfoil produces the maximum thrust at $Re = 185$ and $Sr = 0.4$. Thus, the thickness distribution of the airfoil is also a crucial design parameter for thrust production. When $Sr = 0.2$, the airfoils with the thrust-indicating mushroom vortex patterns behind them do not produce thrust. When $Sr = 0.4$, a phase lag between the indication of the mushroom vortex pattern and the resulting force generation is observed. By investigating the velocity profile and the vorticity intensities in the vortex cores, it can be found that the thrust-indicating mushroom vortex pattern itself cannot guarantee the thrust generation. The thrust-producing airfoil generates the vortices strong enough to overcome the momentum deficit.

Present results are obtained within the limitation of the laminar flow assumption. Numerical schemes that consider the transition from laminar to turbulent flows will be included in the future.

Acknowledgments

The research was supported by a grant from the Academic Research Program of Chungju National University, 2006. This work was also supported by the Korea Research Foundation Grant funded by the Korean Government through the Ministry of Education and Human Resources Development, Basic Research Promotion Fund (KRF-2007-331-D00081).

References

[1] Rozhdestvensky, K. V., and Ryzhov, V. A., "Aerohydrodynamics of Flapping-Wing Propulsors," *Progress in Aerospace Sciences*, Vol. 39, No. 8, 2003, pp. 585–633. doi:10.1016/S0376-0421(03)00077-0

[2] Ho, S., Nassef, H., Pornsinsirirak, N., Tai, Y.-C., and Ho, C.-M., "Unsteady Aerodynamics and Flow Control for Flapping Wing Flyers," *Progress in Aerospace Sciences*, Vol. 39, No. 8, 2003, pp. 635–681. doi:10.1016/j.paerosci.2003.04.001

[3] Sane, S. P., and Dickinson, M. H., "The Aerodynamic Effects of Wing Rotation and a Revised Quasi-Steady Model of Flapping Flight," *Journal of Experimental Biology*, Vol. 205, No. 8, 2002, pp. 1087–1096.

[4] Dickinson, M. H., Lehmann, F.-O., and Sane, S. P., "Wing Rotation and the Aerodynamic Basis of Insect Flight," *Science*, Vol. 284, No. 5422, 1999, pp. 1954–1960. doi:10.1126/science.284.5422.1954

[5] Lehmann, F.-O., "The Mechanisms of Lift Enhancement in Insect Flight," *Naturwissenschaften*, Vol. 91, No. 3, 2004, pp. 101–122. doi:10.1007/s00114-004-0502-3

[6] Wang, Z. J., "Dissecting Insect Flight," *Annual Review of Fluid Mechanics*, Vol. 37, Jan. 2005, pp. 183–210. doi:10.1146/annurev.fluid.36.050802.121940

[7] Mueller, T. J. (ed.), *Fixed and Flapping Wing Aerodynamics for Micro Air Vehicle Applications*, Progress in Astronautics and Aeronautics, Vol. 195, AIAA, Reston, VA, 2001.

[8] Azuma, A., *The Biokinetics of Flying and Swimming*, 2nd ed., AIAA, Reston, VA, 2006.

[9] Shyy, W., Lian, Y., Tang, J., Viieru, D., and Liu, H., *Aerodynamics of Low Reynolds Number Flyers*, Cambridge Univ. Press, New York, 2008.

[10] Triantafyllou, M. S., Techet, A. H., and Hover, F. S., "Review of Experimental Work in Biomimetic Foils," *IEEE Journal of Oceanic Engineering*, Vol. 29, No. 3, 2004, pp. 585–594. doi:10.1109/JOE.2004.833216

[11] Fish, F. E., and Lauder, G. V., "Passive and Active Flow Control by Swimming Fishes and Mammals," *Annual Review of Fluid Mechanics*, Vol. 38, 2006, pp. 193–224. doi:10.1146/annurev.fluid.38.050304.092201

[12] Knoller, R., "Die Gesetze des Lufwiderstandes," *Flug und Motortechnik (Wien)*, Vol. 3, No. 21, 1909, pp. 1–7.

[13] Betz, A., "Ein Beitrag zur Erklarung des Segelfluges," *Zeitschrift fur Flugtechnik und Motorluftschiffahrt*, Vol. 3, 1912, pp. 269–272.

[14] Birnbaum, W., "Das Ebene Problem des Schlagenden Fluegels," *Zeitschrift fuer Angewandte Mathematik und Mechanik*, Vol. 4, No. 4, 1924, pp. 277–292. doi:10.1002/zamm.19240040401

[15] von Kármán, T., and Burgers, J. M., "General Aerodynamic Theory-Perfect Fluids," *Aerodynamic Theory, Division E*, edited by W. F. Durand, Vol. 2, Springer–Verlag, Berlin, 1943.

[16] Jones, K. D., Dohring, C. M., and Platzer, M. F., "Wake Structures Behind Plunging Airfoils: A Comparison of Numerical and Experimental Results," AIAA Paper 1996-0078, 1996.

[17] Jones, K. D., and Platzer, M. F., "An Experimental and Numerical Investigation of Flapping-Wing Propulsion," AIAA Paper 1999-0995, 1997.

[18] Lai, J. C. S., and Platzer, M. F., "Jet Characteristics of a Plunging Airfoil," *AIAA Journal*, Vol. 37, No. 12, 1999, pp. 1529–1537. doi:10.2514/2.641

[19] Platzer, M. F., and Jones, K. D., "Flapping Wing Aerodynamics Progress and Challenges," AIAA Paper 2006-0500, 2006.

[20] Wang, Z. J., "Two Dimensional Mechanism for Insect Hovering," *Physical Review Letters*, Vol. 85, No. 10, 2000, pp. 2216–2218. doi:10.1103/PhysRevLett.85.2216

[21] Wu, J. H., and Sun, M., "Unsteady Aerodynamic Forces of a Flapping Wing," *Journal of Experimental Biology*, Vol. 207, No. 7, 2004, pp. 1137–1150. doi:10.1242/jeb.00868

[22] Miller, L. A., and Peskin, C. S., "When Vortices Stick: an Aerodynamic Transition in Tiny Insect Flight," *Journal of Experimental Biology*, Vol. 207, 2004, pp. 3073–3088. doi:10.1242/jeb.01138

[23] Walker, J. A., "Rotational Lift: Something Different or More of the Same?," *Journal of Experimental Biology*, Vol. 205, No. 24, 2002, pp. 3783–3792.

[24] Shyy, W., and Liu, H., "Flapping Wings and Aerodynamic Lift: The Role of Leading-Edge Vortices," *AIAA Journal*, Vol. 45, No. 12, 2007, pp. 2817–2819. doi:10.2514/1.33205

[25] Childress, S., and Dudley, R., "Transition from Ciliary to Flapping Mode in a Swimming Mollusc: Flapping Flight as a Bifurcation in Re_{ω}," *Journal of Fluid Mechanics*, Vol. 498, 2004, pp. 257–288. doi:10.1017/S002211200300689X

[26] Godoy-Diana, R., Aider, J.-L., and Wesfreid, J. E., "Transitions in the Wake of a Flapping Foil," *Physical Review E (Statistical Physics, Plasmas, Fluids, and Related Interdisciplinary Topics)*, Vol. 77, No. 1, 2008, p. 016308. doi:10.1103/PhysRevE.77.016308

[27] Lentink, D., and Gerritsma, M., "Influence of Airfoil Shape on Performance in Insect Flight," AIAA Paper 2003-3447, 2003.

[28] Sun, M., and Tang, J., "Unsteady Aerodynamic Force Generation by a Model Fruit Fly Wing in Flapping Motion," *Journal of Experimental Biology*, Vol. 205, No. 1, 2002, pp. 55–70.

[29] Wang, Z. J., "Vortex Shedding and Frequency Selection in Flapping Flight," *Journal of Fluid Mechanics*, Vol. 410, 2000, pp. 323–341. doi:10.1017/S0022112099008071

[30] Freymuth, P., Gustafson, K. E., and Leben, R., "Visualization and Computation of Hovering Mode Vortex Dynamics," *Vortex Method and Vortex Motion*, edited by K. Gustafson, and J. Sethian, Society for Industrial and Applied Mathematics, Philadelphia, 1991.

[31] Taylor, G. K., Nudds, R. L., and Thomas, A. L. R., "Flying and Swimming Animals Cruise at a Strouhal Number Tuned for High Power Efficiency," *Nature*, Vol. 425, Oct. 2003, pp. 707–711. doi:10.1038/nature02000

[32] Bhatnagar, P. L., Gross, E. P., and Krook, M., "A Model for Collision Processes in Gases: Small Amplitude Processes in Charged and Neutral One-Component System," *Physical Review*, Vol. 94, No. 3, 1954, pp. 511–525. doi:10.1103/PhysRev.94.511

[33] Chen, S., and Doolen, G., "Lattice Boltzmann Method for Fluid Flows," *Annual Review of Fluid Mechanics*, Vol. 30, 1998, pp. 329–364. doi:10.1146/annurev.fluid.30.1.329

[34] Chapman, S., and Cowling, T. G., *The Mathematical Theory of Nonuniform Gases*, 3rd ed., Cambridge Univ. Press, New York, 1970.

[35] Lallemand, P., and Luo, L.-S., "Lattice Boltzmann Method for Moving Boundaries," *Journal of Computational Physics*, Vol. 184, No. 2, 2003, pp. 406–421. doi:10.1016/S0021-9991(02)00022-0

[36] Mei, R., Yu, D., Shyy, W., and Luo, L.-S., "Force Evaluation in the Lattice Boltzmann Method Involving Curved Geometry," *Physical Review E (Statistical Physics, Plasmas, Fluids, and Related Interdisciplinary Topics)*, Vol. 65, No. 041203, 2002, pp. 1–14.doi: 10.1103/PhysRevE.65.041203

[37] Guilmineau, E., and Queutey, P., "A Numerical Simulation of Vortex Shedding from an Oscillating Circular Cylinder," *Journal of Fluids and Structures*, Vol. 16, No. 6, 2002, pp. 773–794. doi:10.1006/jfls.2002.0449

[38] Kim, D., and Choi, H., "Immersed Boundary Method for Flow Around an Arbitrarily Moving Body," *Journal of Computational Physics*, Vol. 212, No. 2, 2006, pp. 662–680. doi:10.1016/j.jcp.2005.07.010